RESEARCH PAPER

Synthesis and Characterization of Organo-Polymeric Hybrid Nanocomposite as a Dielectric Material

Hayder H. Ahmed, Zaid H. Mahmoud *, Jinan Mohammed Mahmood*

Chemistry Department, College of Sciences, University of Diyala, Iraq

ARTICLE INFO

Article History:
Received 05 October 2025
Accepted 19 March 2026
Published 01 April 2026

Keywords:
DSC
In situ polymerization
Hybrid
Nanocomposite
TGA

ABSTRACT

Pure and different weight ratio of Cu-complex incorporated polypyrrole have been successfully prepared employing in situ polymerization of pyrrole solution with Cu-complex. The structure, morphology, optical and thermal characterization were carried out by X-ray diffraction (XRD), transmission electron microscopy (TEM), UV-Visible spectrophotometer (UV-Vis) and thermogravimetric analysis (TGA). The XRD results appear preparation amorphous polypyrrole and it amorphousity was reduced with doped Cu-complex. TEM images show preparing spherical nanoparticles of Cu-complex that covered rod morphology of polypyrrole and successfully process of in situ polymerization. on the other hand, the thermal stability of polypyrrole was increased with incorporation Cu-complex as demonstrated from TGA measurements. LCR measurements are appeared that the real and imaginary dielectric constant of hybrid nanocomposite is larger than pure polypyrrole and the storage charges increase with increasing the Cu-complex concentration.

How to cite this article
Ahmed H., Mahmoud Z., Mahmood J. Synthesis and Characterization of Organo-Polymeric Hybrid Nanocomposite as a Dielectric Material. J Nanostruct, 2026; 16(2):1890-1899. DOI: 10.22052/JNS.2026.02.038

INTRODUCTION

Recently, many of works on Schiff bases and its complexes are explored according to its implementations in sensor device and using its as dielectric materials [1,2]. Now, a new area of research or works contain utilizing polymertic compounds is appearing and having significant tension. The prepare of polymers, which contain nanometric materials, is deem an integral part of polymer technology and presence of these organic materials enter polymer structure have been enhanced essentially features other than pure polymer [3,4]. There are many papers carried out on the field of storage of charges, so this field be current face of works and had the characteristic interest in electric technologies according to its features like low cost, excellent promising physical and chemical properties [5]. Many oxides were used as dielectric materials and many works reported success of it in this fields [6-8]. Bashir et al., reported used of Fe_3O_4 that synthesized hydrothermally as dielectric materials and its showed 118 F/g at 6 mA [9], while Brousse shown that same oxide electrode appeared ability of 75 F/g specific capacitance [10]. However, due to the redox kinetics are reserved via transfer of electrons and mass diffusion, this oxide type has a smaller cycles life. For this, the authors notice was drawn to hybrid materials due to their long cyclic life, high voltage and energy density [11]. These materials conduct well in energy storage field. The organic/polymer nanocomposite

* *Corresponding Author Email: dorkoosh@tums.ac.ir*

compounds have different properties than pure polymeric compounds because of their properties such as surface area, transfer of lone pairs inside the polymer chain and chemical structure [12]. In this work, we discussed the energy storage behavior of copper complex/poypyrrole hybrid nanocompsoite that appear excellent storage properties compare with pure polypyyrole, making it as an elect for potential utilize in supercapacitor application.

MATERIALS AND METHODS

All chemical materials were supplied from Sigma-Aldrich and used without future purification

synthesis of ligand and copper complex

Firstly, (1.741 g, 0.01 mole) of (4-H-1-Benzopyran-3-carboxaldehyde) was dissolved in (20 ml) ethanol in 50 ml the beaker, then (6 drops) of glacial acetic acid were added to it and left for 20 min (sol. 1). Then, in another beaker, (1.001 g) of (2-amino benzothiazole) was added to 20 ml of ethanol (sol. 2). The two solutions were mixed by adding the sol. 2 to 1 with continuous stirring. After that, the mixture was refluxed at 80 °C for 15h continuously until it got a yellow precipitate. Finally, it filtered, washed and dried at room temperature. Its weight was (2.15 g), meaning its percentage was (70.261%). Separately, (1mmol, 0.306g) of 4-H-1-Benzopyran-3-carboxaldehyde and (1mmol, 0.241g) of copper nitrate were dissolved in (10 ml) of hot ethanol. Then, the two solutions were mixed under a continuous stirrer. After that, the mixture was refluxed at 80 °C for 4 h. Finally, it was filtered, washed, and dried at room temperature. The weight of the product was (0.974g).

Preparation of polypyrrole, Cu-complex doping polypyrrole and its films

(3 ml) of pyrrole was mixed with (20 ml) of HCl acid (0.5M) in an ice bath. The mixture was then dropped by (2M, 20 ml) ammonium persulfate (APS). The black precipitate formed was placed in the refrigerator for 24 h. The product was then filtered and washed several times until the solution became transparent (PH=7). For doping process, 0.01 g of Cu-complex, 3 ml of pyrrole were mixed with (20 ml) of HCl acid (0.5M) in an ice bath. The mixture was then dropped by (2M, 20 ml) ammonium persulfate (APS). The black precipitate formed was placed in the refrigerator for 24 h. The product was then filtered and washed several times until the solution became transparent (PH=7). For preparation its films, (0.01g) of PPy was sonicated with 5ml ethanol to get a homogenous solution. Then, it was mixed with (5ml, 2%) PVA solution under a contentious

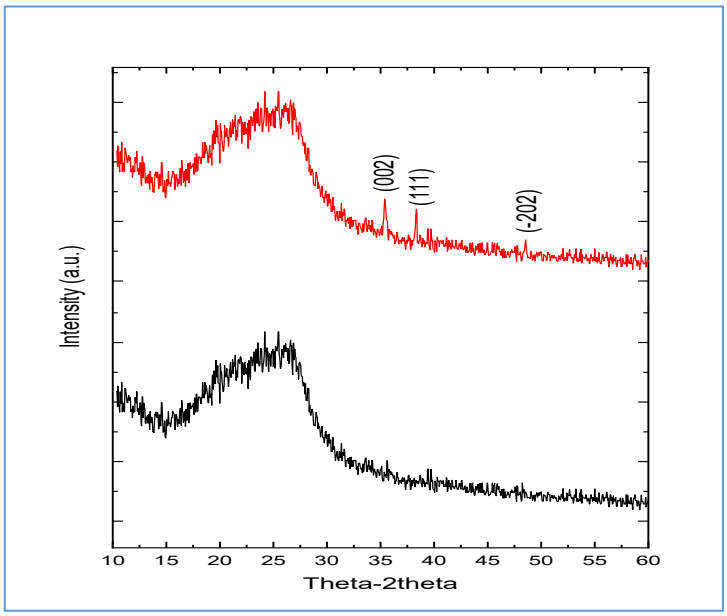

Fig. 1. XRD of pure and Cu-complex doped PPy.

stirrer for 2 h. After that, the mixture was cast into a glassy mold. Finally, it was left for 36 h to dry at room temperature before taking it for LCR measurement. The producer was repeated with (0.01-0.05g) of Cu-complex/PPy.

RESULTS AND DISCUSSION

The structural, crystalline phase, size and formation of polypyrrole were determined by using XRD analysis. Fig. 1 shows the XRD pattern of pure and Cu-complex incorporated polypyrrole (PPy). The results illustrated a broad characteristic diffraction peak with a range of 2q 20-30, which indicated the amorphous nature of the prepared polymer [13], which is attributed to the scattering of chains at the interplanar spacing [14]. On the other hand, For Cu-complex incoprted PPy, the results appear to be a broad diffraction peak located at 20-30 assigned to a repeated chain of PPy and three diffraction peaks centered at 2θ = 35.44, 38.56, and 48.52o that index to (002), (111), and (-202) planes of Cu-complex.

The results of incorporating PPy nanocomposite revealed a broad diffraction peak of PPy located at 20-30, which indicates the polymer's amorphous nature remained until after adding the oxides and metal through the crystal lattice, which implies that it retained its identical structure. On the other hand, the results showed decreasing the intensity diffraction peaks of PPy after incorporating with Cu-complex, which may be due to the complex significantly reducing the amorphous nature of PPy polymer [15]. When comparing the broad diffraction peak of pure and incorporating PPy, it was noted to be a little shifted in because adding complex works in inducing the strain in the PPy matrix, as well as the strong interaction between the polar segment of PPy and orbital in Cu-complex [16]. The interaction between PPy chains with complex can be discuss from investigation of chain separation of PPy by using the following Eq. 1 [17]:

$$R = \frac{8\lambda}{3\sin\theta} \quad (1)$$

The results appear that the incorporated material doesn't noticeably alter the interplanar distance. It also leads to the production of a more compact structure of nanocomposite because of the interaction between oxides/metal and the active group of PPy [18].

The morphology of pure and Cu-complex incorporation with PPy was investigated using TEM and the results are shown in Fig. 2a and b. Fig. 2a show TEM images of PPy synthesized by oxidative polymerization using ammonium persulfate as initiators. The results appear to show that the morphology of PPy is nanotubes have been formed at the nanoscale. Fig. 2b shows the uniform distribution of spherical Au nanoparticles within PPy matrix, which indicate successfully synthesized of Au/PPy nanocomposite.

Analyzing optical absorption spectra is

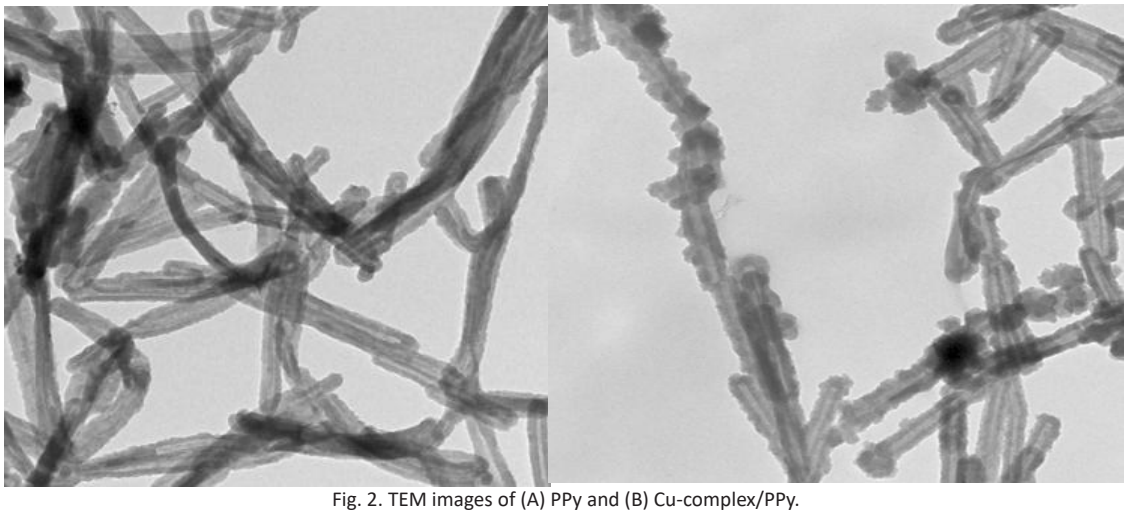

Fig. 2. TEM images of (A) PPy and (B) Cu-complex/PPy.

the most efficient method for enhancing and comprehending amorphous materials' structure and energy gap. The adsorption spectra of PVA/PPy with different concentrations of Cu-complex are shown in Fig. 3a. The results shown a band shoulder at around 270 nm that could be attributed to n → π*, which could originate from O–H [19]. On the other hand, the results showed that the PVA/PPy intensities are reduced with increasing Cu-complex concentrations in the nanocomposite and shifting in the shoulder peaks for a lower wavelength, which confirmed the interaction between the Cu with active groups in the polymer and this interaction become more effective with increasing Cu-complex concentration [20]. The band gap of pure and PVA/PPy doped by Cu-

Table 1. direct and indirect band gap of PVA/PPy-wt.% CuL2.

Materials	Band gap (eV)	
	Direct	Indirect
PVA/PPy	5.13	4.93
PVA/PPy-0.01wt.% CuL_2	5.03	4.86
PVA/PPy-0.02wt.% CuL_2	4.95	4.73
PVA/PPy-0.03wt.% CuL_2	4.92	4.66
PVA/PPy-0.05wt.% CuL_2	4.72	4.30

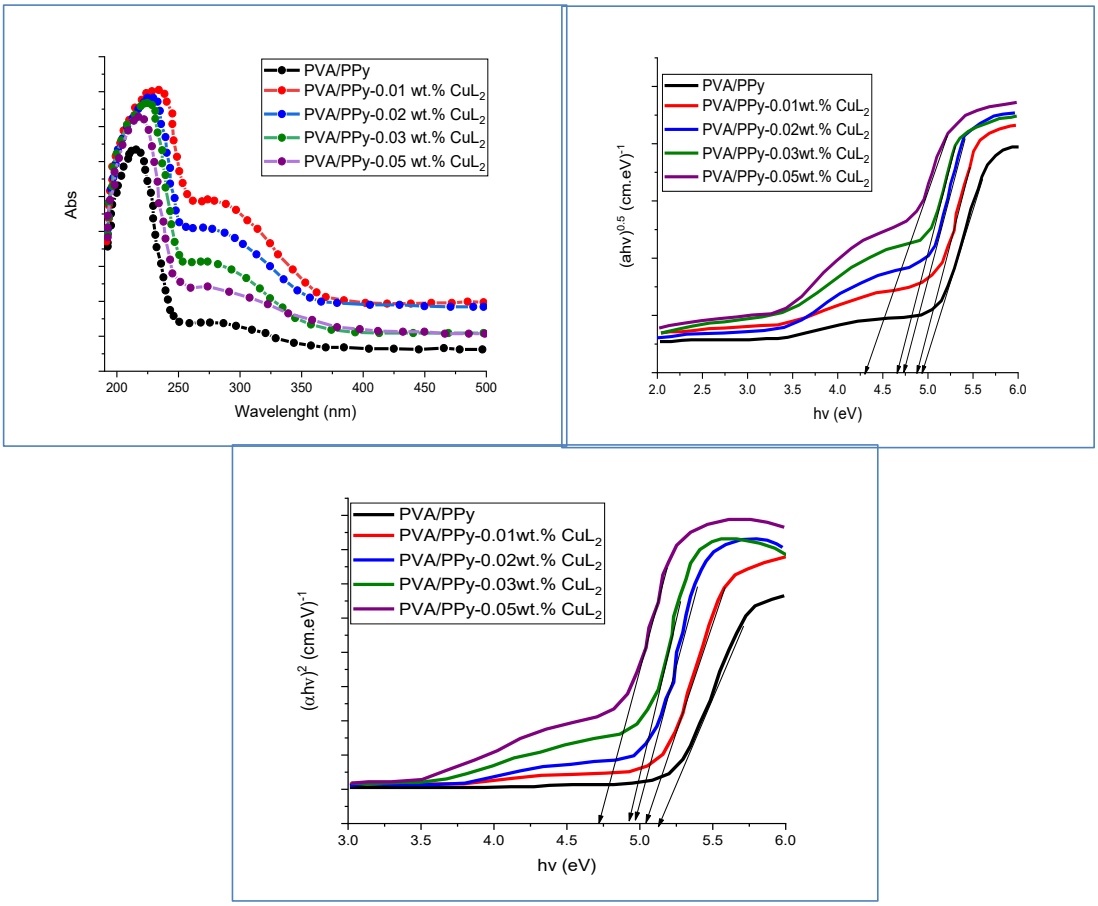

Fig. 3. (a) UV-Vis of pure and Cu-complex doped PPy, (b) direct band gaps and (c) indirect band gap.

complex is investigated via UV-Vis spectra by using the Tauc plot given from the following Eq. 2 and 3 [21]:

$$(\propto hv)^{0.5} = B^{0.5}(hv - E_g^{in}) \quad (2)$$

$$(\propto hv)^{2} = B^{2}(hv - E_g^{d}) \quad (3)$$

Where: h is Planck constant, Eg, band gap, α absorption coefficient, and B is constant. The α can be investigated as a photon frequency function via the following Eq. 4:

$$\propto = 2.303(\frac{A}{d}) \quad (4)$$

where d is the film thickness, A represents absorbance, and n is the factor of the exponent. The values of the band gap were investigated for PVA/PPy incorporated Cu-complex via plotting $(\alpha hv)^2$ and $(\alpha hv)^{1/2}$ for direct and indirect transition as demonstrated in Fig. 3b and c. The results show that doping Cu-complex in the matrix of PPy reduces band gaps because of the generation of defects in nanocomposites. These defects cause the localized state in the band gap that replicates the degree of disorder in prepared materials and can be the reason for the reaction between the chain of PPy and the Cu-complex. The results of band gaps are tabled in Table 1.

The thermal of PVA/PPy and PVA/PPy incorporating Cu-complex are investigated by DTA analysis, and the results are shown in Fig. 4a. The results demonstrated the shifting of the melting temperature (Tm) by incorporating Cu-complex according to the PAV/PPy with different concentrations of Cu-complex. The PVA/PPy mixture appears as a single Tm at 260 °C, which indicates the good mixing or miscibility between them [22] due to producing an H-bond between the functional groups in polymers. On the other hand, it is noted that the Tm was shifted to a higher temperature with increasing Cu-complex concentration because of enhancing the nanocomposite's thermal stability after adding Cu-complex. In addition, the endothermic peaks between 250 to 330 °C for PVA/PPy and PVA/PPy incorporating Cu-complex appear to be the semicrystalline nature of prepared compounds. These results are in agreement with XRD results. The thermal stability and kinetic parameters of PPy and PPy incorporated with Cu-complex were investigated by TGA and entry from 30 to 600 °C, as shown in Fig. 4b. The results showed three losses of weight or decompositions in all curves. The first loss occurs in the 33 to 140 °C range, assigned to the evaporation of the PVA/PPy matrix with the associated solvent [23]. The second loss begins in the 140.5 to 320 °C range, which returns to the active group decomposition. The third loss

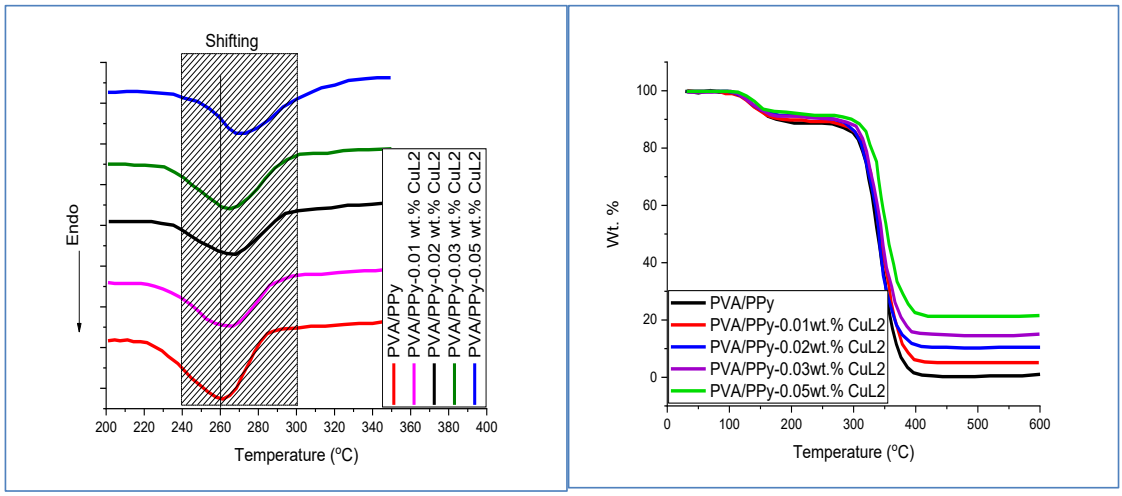

Fig. 4. (A) DSC and (B) TGA of PVA/PPy and PVA/PPy incorporated Cu-complex.

is exhibited at 380 and extended to 600 °C, which is assigned to the degradation of PVA/PPy polymer chains. On the other hand, the results appear a considerable enhancement in the thermal stability of the polymer with Cu-complex incorporation compared with the blend sample because of the interaction between the PVA/PPy and Cu-complex complex [24].

The activation energy of PVA/PPy and PVA/PPy incorporated Cu-complex were estimated by TGA analysis by using the Coats-Redfern method by using the following Eq. 5:

$$\mathrm{Log}[\frac{1-(1-\alpha)^{1-n}}{T^2}] = \log\frac{R}{\Delta E}\left[1-\frac{2RT}{E}\right]-\frac{Ea}{2.303RT} \quad (5)$$

Where α is the degree of decomposition, and is found as follows:

$$\alpha = \frac{mi - mt}{mi - mf} \quad (6)$$

The activation energy of prepared compounds can be calculated by plotting -Log [1-(1-α)/T^2] versue 1000/T and estimating from following Eq. 7:

$$Ea = 2.303R.\,slope \quad (7)$$

The results (Table 2) showed that the activation energy is reduced gradually from 355 to 313 Kcal/mol with increasing the Cu-complex incorporating concentration, which may be back to producing the defects created through the reaction between the PPy chains with Cu-complex and the production of new bonds.

The real and imaginary permittivity of pure and PVA loaded by Cu-complex and ligand films were measured as a function of frequency at (10 kHz-1 MHz). The results were calculated using the following Eqs. 8 and 9 [25]:

$$\varepsilon' = \frac{C \times d}{\varepsilon_\circ \times A} \quad (8)$$

$$\varepsilon'' = \tan\sigma * \varepsilon' \quad (9)$$

Where: c: the capacitance, d: the thickness of the film, A: the area of cross section and $\varepsilon_\circ$: the permittivity of free space ($8.85*10^{-12}$ F/m). The results are shown in Fig. 5a and b. All synthetic dielectric materials studies demonstrate that, due to the polarization mechanism, the real and imaginary dielectric decreases with increasing frequency [26]. The dielectric constant in the dielectric analysis depends upon the dipolar relaxation at high frequency and the interfacial polarization at low frequency [27]. Strong interfacial polarization is primarily responsible for the high dielectric constant values at low frequencies that arise from applying an electric field to a material, which causes charges to accumulate between conductive and insulating regions. On the other hand, the rapid variation of dipoles to align themselves is responsible for the decreasing dielectric constant values at high frequencies. The observed variation in the real and imaginary dielectric constant values as a function of frequency is ascribed to the dipole polarization of isolated polarons and bipolarons. Two equilibrium positions are used to record the dipole rotation. The spontaneous alignment of the dipoles at one position indicates the nonlinear polarization behavior of the synthesized nanocomposite, and the results indicate a change

Table 2. The activation energy values of PVA/PPy-wt.% Cu-complex.

No.	PVA/PPy (Cu-complex wt.%)	Ea Kcal/mol
1	PVA/PPy	355.54
2	PVA/PPy-1wt.% CuL2	345.89
3	PVA/PPy-2wt.% CuL2	333.11
4	PVA/PPy-3wt.% CuL2	324.07
5	PVA/PPy-5wt.% CuL2	313.15

in the dielectric constant values [28].

When PPy/PVA dielectric constant results are compared with and without adding complexes nanoparticles, low real dielectric constant values are obtained at low frequencies and stay low with increasing frequency for PVA loaded by PPy as shown in Fig. 6a and b. In contrast, high real dielectric constant values are obtained at low frequencies after the addition of oxide ligands and their complexes nanoparticles, which may be due to increased charge carrier localization along with polarons, leading to higher AC conductivity. The real dielectric constant at low frequency may rise for any of the previously listed reasons [29]. Contrarily, conducting polymers are semi-crystalline materials of distinct crystalline regions due to chain folding by amorphous barriers. Maxwell–Wagner-Sillars (MWS) polarization, also known as interfacial polarization, results from charge carrier accumulation at the interfaces between crystalline and amorphous regions in pure blends, which causes a rise in dielectric permittivity [30]. The PVA/PPy-Cu complex system is a heterogeneous combination of PVA/PPy and

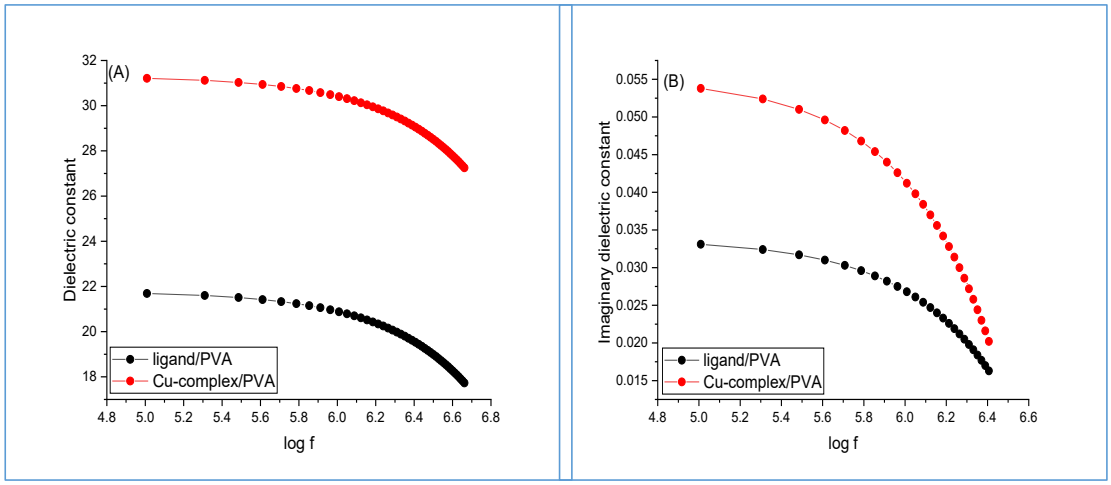

Fig. 5. (A) real and (B) imaginary dielectric constant of ligand and Cu-complex.

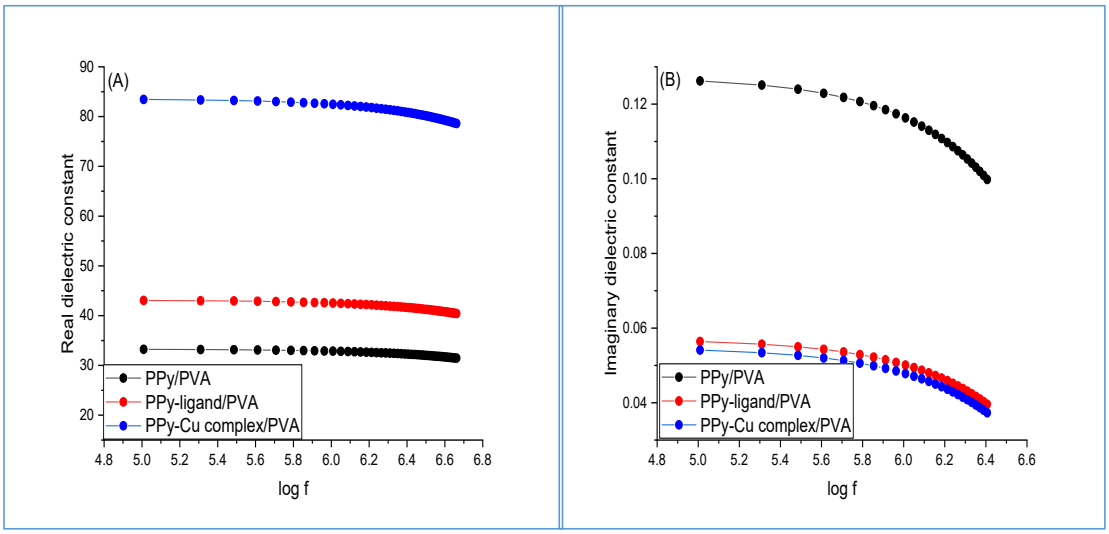

Fig. 6. (A) real and (B) imaginary dielectric constant of pure and ligand Cu-complex doped PPy.

complex, with elements that differ in permittivity and conductivity. As a result, space charges grow at those macroscopic interfaces where an electric field is applied [31]. The MWS effect depends on the conductivity and permittivity of the compound material's constituents, which produce greater dielectric constant values at low frequencies. It arises from the accumulation of charges on the interfaces inside the bulk of the sample, generating enormous dipoles. In addition, electrode polarization also plays a role in maintaining dielectric stability at low frequencies [32]. As copper complexes are incorporated, dielectric permittivity values also rise because the doping of Cu-complex into the PVA/PPy matrices increases the interfacial area between the complex and PVA/PPy. When an Ac field is applied, more charge carriers are inhibited within these interfaces, which raises the MWS polarization. Incorporating complexes into systems also made the system more heterogeneous, which increased the number of interfaces between complex and PVA/PPy and raised the dielectric permittivity values. It is evident at high frequencies that the dielectric permittivity value decreases steadily as the frequency increases. This phenomenon is attributed to interfacial dielectric relaxation or space charge polarization effects.

The dielectric constant of pure and different weight ration of Cu-complex incorporated polypyrrole is demonstrated in Fig. 7. The results appear considerable enhanced the real dielectric value with increasing the concentration ratio of complex until 0.04 wt.% of nanocomposite, which may be to the interaction between the Cu-complex and polar fraction of polypyrrole that responsible for high value of constant [33], as well as, the interfacial polarization enhanced enter the hybrid composite is high at 0.04 wt.%. On the other side, the results appeared reducing in dielectric constant at 0.05 wt.% which may be assign to the lower interaction between the complex and the polypyrrole chain that produced an inhomogeneity [34]. In addition to, the formation of voids inside the polymer chain causes to reduce the charges movement, hence reducing the real dielectric

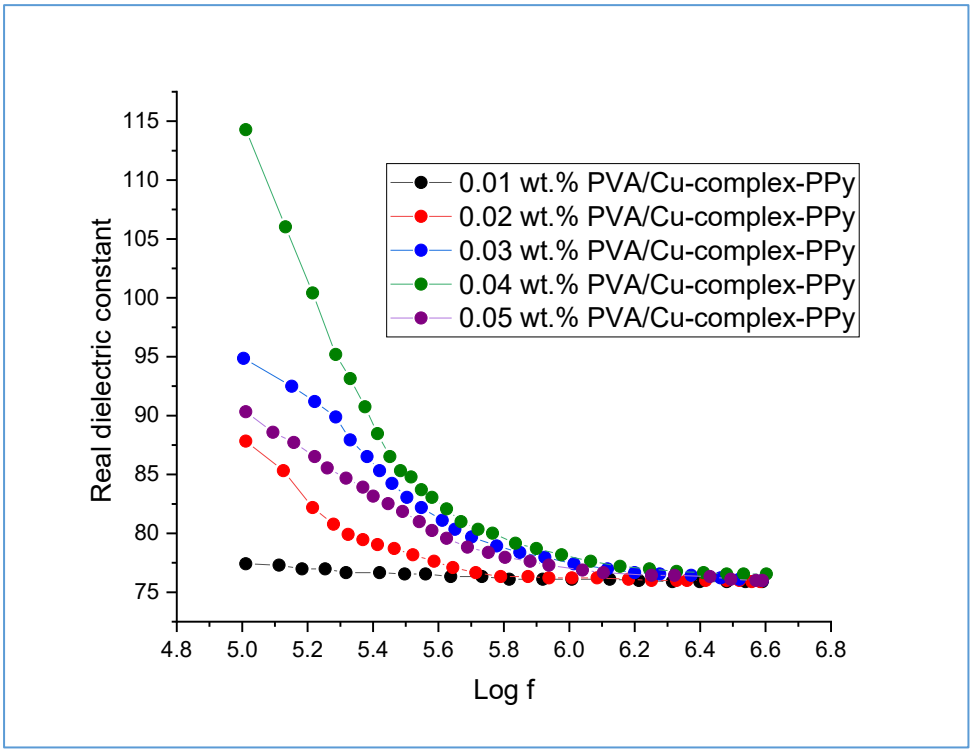

Fig. 7. Real dielectric constant of wt.% Cu-complex doped PPy.

constant value at 0.05 wt.% of filler particles.

CONCLUSION

In this work, an in situ is used to the polymerization different weights ratio of Cu (4-H-1-Benzopyran-3-carboxaldehyde) complex with PPy during oxidative polymerization form PVA/Cu-complex-PPy hybrid nanocomposite and it characterized via varied techniques such as XRD, TEM, DSC, TGA and UV-Vis before energy storage measurements. The LCR measurements exhibit the pseudocapacitive nature of PVA/Cu-complex-PPy.

CONFLICT OF INTEREST

The authors declare that there is no conflict of interests regarding the publication of this manuscript.

REFERENCES

1. Mahmoud ZH, Hammoudi OG, Abd AN, Ahmed YM, Altimari US, Dawood AH, et al. Functionalize cobalt ferrite and ferric oxide by nitrogen organic compound with high supercapacitor performance. Results in Chemistry. 2023;5:100936.
2. Mustafa MA, Qasim QA, Mahdi AB, Izzat SE, Alnassar YS, Abood ES, et al. Supercapacitor Performance of Fe3O4 and Fe_3O_4@SiO_2-bis(aminopyridine)-Cu Hybrid Nanocomposite. International Journal of Electrochemical Science. 2022;17(10):221057.
3. Mahmoud ZH, Al-Bayati RA, Khadom AA. In situ Polymerization of Polyaniline/Samarium Oxide - Anatase Titanium Dioxide (PANI/TiO_2) Nanocomposite: Structure, Thermal and Dielectric Constant Supercapacitor Application Study. Journal of Oleo Science. 2022;71(2):311-319.
4. Mansoor Al Sarraf AA, H. Alsultany F, H. Mahmoud Z, S. Shafik S, I. Ai Mashhadani Z, Sajjadi A. Magnetic nanoparticles supported zinc (II) complex (Fe_3O_4@SiO_2-Imine/Thio-$Zn(OAc)_2$): a green and efficient magnetically reusable zinc nanocatalyst for synthesis of nitriles via cyanation of aryl iodides. Synth Commun. 2022;52(9-10):1245-1253.
5. Mahmood JM, Mahmoud ZH, Al-Obaidi NS, Rahima AM. Gama-Fe_2O_3 silica-coated 2-(2-benzothiazolyl azo)-4-methoxyaniline for supercapacitive performance. Journal of Electrochemical Science and Engineering. 2023;13(3):521-536.
6. Hsu C-Y, Ajaj Y, Ghadir GK, Al-Tmimi HM, Alani ZK, Almulla AA, et al. Rechargeable batteries for energy storage: A review. e-Prime - Advances in Electrical Engineering, Electronics and Energy. 2024;8:100510.
7. Mahmoud ZH, Ajaj Y, Kamil Ghadir G, Musaad Al-Tmimi H, Hameed Jasim H, Al-Salih M, et al. Carbon-doped titanium dioxide (TiO_2) as Li-ion battery electrode: Synthesis, characterization, and performance. Results in Chemistry. 2024;7:101422.
8. Jawad AaA, Mahmoud ZH, Kadhim MM, Rheima AM, Abbas ZS, Al-bayati ADJ, et al. Functionalize and supercapacitor performance of magnetic oxide nanoparticles. Inorg Chem Commun. 2023;154:110884.
9. Bashir S, Manogran P, Goh ZL, Elizer NR, Ramesh K, Ramesh S. Metal Oxide-based Nanocomposites for High-Energy Applications. Advancements in Nanomaterials for Energy Conversion and Storage: CRC Press; 2024. p. 146-168.
10. Brousse T, Bélanger D. A Hybrid Fe_3O_4]-MnO_2] Capacitor in Mild Aqueous Electrolyte. Electrochem Solid-State Lett. 2003;6(11):A244.
11. Mahmoud ZH, Al-Bayati RA, Khadom AA. Synthesis and supercapacitor performance of polyaniline-titanium dioxide-samarium oxide (PANI/TiO_2-Sm_2O_3) nanocomposite. Chemical Papers. 2021;76(3):1401-1412.
12. Mahmoud ZH, Al-Bayati RA, Khadom AA. Electrochemical Photocatalytic Degradation of Rhodamine B Dye by Sm^{3+} doped Titanium Dioxide (Sm-TiO2) in Natural Sunlight Exposure. International Journal of Electrochemical Science. 2021;16(12):211241.
13. Hussain S, Tahir M, Ibraheem, Ali S, Muhammad F, Gul Z, et al. Polypyrrole: synthesis, characterization and its potential application for humidity sensor. Polym Bull. 2024;81(10):8869-8882.
14. Mahmood J, Arsalani N, Naghash-Hamed S, Hanif Z, Geckeler KE. Preparation and characterization of hybrid polypyrrole nanoparticles as a conducting polymer with controllable size. Scientific Reports. 2024;14(1).
15. Malook K, Ihsan ul H, Khan M, Ali M. Polypyrrole-CuO based composites, promotional effects of CuO contents on polypyrrole characteristics. Journal of Materials Science: Materials in Electronics. 2019;30(4):3882-3888.
16. Helli M, Sadrnezhaad SK, Hosseini-Hosseinabad SM, Vahdatkhah P. Synthesis and characterization of CuO micro-flowers/PPy nanowires nanocomposites as high-capacity anode material for lithium-ion batteries. J Appl Electrochem. 2023;54(1):1-11.
17. Zhang Q, He X-H. Phase Separation of Polymer Blends Induced by an External Static Electric Field. Chin J Polym Sci. 2022;41(6):972-980.
18. Kobayashi Y, Ishida S, Ihara K, Yasuda Y, Morita T, Yamada S. Synthesis of metallic copper nanoparticles coated with polypyrrole. Colloid Polym Sci. 2009;287(7):877-880.
19. Khan H, Malook K, Shah M. Polypyrrole/MnO2 composites: synthesis, structural and electrical properties. Journal of Materials Science: Materials in Electronics. 2018;29(11):9090-9098.
20. Elashmawi IS, Ismail AM, Abdelghany AM. The incorporation of polypyrrole (PPy) in CS/PVA composite films to enhance the structural, optical, and the electrical conductivity. Polym Bull. 2022;80(10):11379-11399.
21. Jubu PR, Obaseki OS, Ajayi DI, Danladi E, Chahrour KM, Muhammad A, et al. Considerations about the determination of optical bandgap from diffuse reflectance spectroscopy using the tauc plot. Journal of Optics. 2024;53(5):5054-5064.
22. Rowe AA, Tajvidi M, Gardner DJ. Thermal stability of cellulose nanomaterials and their composites with polyvinyl alcohol (PVA). J Therm Anal Calorim. 2016;126(3):1371-1386.
23. Reguieg F, Ricci L, Bouyacoub N, Belbachir M, Bertoldo M. Thermal characterization by DSC and TGA analyses of PVA hydrogels with organic and sodium MMT. Polym Bull. 2019;77(2):929-948.
24. Karthik S, Suresh J, Thangaraj V, Balaji K, Selvasekarapandian S, Shanmugasundaram S, et al. Electrical and mechanical property of the polyvinyl alcohol based solid electrolyte film contains alum. SN Applied Sciences. 2019;1(11).

25. Orlandi MO, Ramirez MA, Foschini CR, Felix AA, Varela JA. Giant Dielectric Constant Materials and Their Applications. Sol-Gel Processing for Conventional and Alternative Energy: Springer US; 2012. p. 123-146.
26. Li Y, He M. Recent advancements in achieving high dielectric constant polymer dielectrics for low-power-consumption organic field-effect transistors. MRS Communications. 2024;14(2):167-177.
27. Yuan J, Yao S, Poulin P. Dielectric Constant of Polymer Composites and the Routes to High-k or Low-k Nanocomposite Materials. Polymer Nanocomposites: Springer International Publishing; 2016. p. 3-28.
28. Smith BL. Relation of the Dielectric Constant and the Refractive Index to Thermodynamic Properties. Experimental Thermodynamics Volume II: Springer US; 1968. p. 579-606.
29. Srivastava D, Shukla RK. Dielectric Properties of PAni/ZnO Composite. Springer Proceedings in Physics: Springer Singapore; 2019. p. 323-327.
30. Sharanappa N, Mallinath P. Study of dielectric properties of Al_2O_3 doped polyaniline. Sādhanā. 2023;48(3).
31. Paul SJ, Gupta BK, Chandra P. Probing the electrical and dielectric properties of polyaniline multi-walled carbon nanotubes nanocomposites doped in different protonic acids. Polym Bull. 2020;78(10):5667-5683.
32. Basavaraj B, Sannakki B. Investigations on dielectric properties of polymer nanocomposites of PANI/Fe_2O_3. Bull Mater Sci. 2021;44(3).
33. Wang Q, Wu W, Che J, Chen T, Liu X, Huai K, et al. High dielectric PANI/PDMS all-organic composites fabricated by electric fields-assisted assembling. Polym Bull. 2022;80(11):12417-12431.
34. Naqash W, Majid K. Synthesis and characterisation of a high dielectric constant and ac-conducting PANI/$[Co(NH_3)_3(C_4H_4N_2)_3]Cl_3$ nanocomposite. Journal of Materials Science: Materials in Electronics. 2017;28(24):18322-18330.